Upscaling of reactive mass transport in fractured rocks with multimodal reactive mineral facies

Hailin Deng,[1,2] Zhenxue Dai,[1] Andrew Wolfsberg,[1] Zhiming Lu,[1] Ming Ye,[2] and Paul Reimus[1]

Received 6 July 2009; revised 18 November 2009; accepted 16 December 2009; published 4 June 2010.

[1] This paper presents a methodology for upscaling matrix-material transport parameters in fractured-flow dominated systems with multimodal reactive mineral facies. The upscaling method provides a theoretical and practical link between controlled experimental results at the laboratory/bench scale and multikilometer field scales at which contaminant remediation and risk assessment are actually conducted. As sorption reactions in matrix are in part determined by mineral properties, a new conceptual model is developed to reflect the hierarchical structure of reactive mineral facies at the microform, mesoform, and macroform scales. The conceptual model of hierarchical reactive matrix mineral facies is integrated with a dual-porosity model for simulating diffusion of solutes out of fractures and sorption onto the matrix minerals. By assuming that sorption reactions primarily occur in the rock matrix, we develop a multimodal spatial random function for characterizing both the tortuosity (physical heterogeneity) and sorption coefficient (chemical heterogeneity) at different scales in the rock matrix. The effective tortuosity at the field scale is derived by volume averaging of mass transfer coefficient for a conservative species. Subsequently, using a sorbing species (e.g., uranium), we derive the equations for upscaling the sorption coefficients in a saturated, fractured-rock system for field-scale simulations. The effective field-scale tortuosity and sorption coefficient are related to their mean, variance, integral scale, and domain size along a pathway through a three-dimensional flow field. The upscaled values increase with the integral scale and are larger than their geometric mean. Simulations conducted with upscaled sorption coefficients and tortuousities are compared very well with high-resolution Monte Carlo simulations capturing the parameter spatial variations. Results of this study can be extended to explore scale dependence of other important transport parameters for fractured-rock solute transport.

Citation: Deng, H., Z. Dai, A. Wolfsberg, Z. Lu, M. Ye, and P. Reimus (2010), Upscaling of reactive mass transport in fractured rocks with multimodal reactive mineral facies, *Water Resour. Res.*, *46*, W06501, doi:10.1029/2009WR008363.

1. Introduction

[2] A significant challenge in groundwater flow and reactive transport modeling is to develop scale-appropriate parameters to represent physical and chemical heterogeneities that impact solute migration estimates. Upscaling of transport parameters for porous media has been studied for decades, and various upscaling methods have been developed [*Cushman et al.*, 2002, and references therein]. Upscaling transport parameters for fractured porous media presents particular challenges due to the medium complexity and heterogeneity [*Tsang and Neretnieks*, 1998; *Steefel et al.*, 2005; *Neuman*, 2005]. In fractured-rock systems, the mass transfer coefficient which quantifies the mass transfer between fracture and matrix is one of the most important transport parameters because it links both physical heterogeneity (reflected through tortuosity and diffusion) and chemical heterogeneity (through sorption coefficient). In practice, it is not uncommon that the values of tortuosity and sorption coefficient measured from column experiments are used directly, without upscaling, for field-scale reactive transport modeling [*Dai et al.*, 2009]. However, without using scale-justified effective parameters, field-scale modeling may lead to inaccurate simulations of physical and chemical processes.

[3] The retardation of a solute relative to the fracture flow velocity is due to diffusion out of fractures and sorption on matrix minerals. Multiple factors affect these processes, including the fracture aperture, the fracture volume fraction, the matrix porosity and tortuosity, and the type and surface area of matrix minerals. In this study, we focus on matrix material tortuosity and the sorption coefficient for heterogeneous physical and chemical processes, respectively, along a migration pathway. Since the matrix sorption coefficient is closely related to mineral properties, scaling behaviors of the sorption coefficient can be explained by studying the spatial variability of reactive mineral facies at different scales [*Zavarin et al.*, 2004; *Allen-King et al.*, 2006; *Dai et al.*, 2009]. A systematic quantification method for

[1]Earth and Environmental Sciences Division, Los Alamos National Laboratory, Los Alamos, New Mexico, USA.
[2]Department of Scientific Computing and Department of Geological Sciences, Florida State University, Tallahassee, Florida, USA.

0043-1397/10/2009WR008363

upscaling the sorption coefficient based on mineral spatial distributions is needed to link the distributions of reactive minerals in the field-scale modeling to lab column-scale measurements. In this study, a new methodology is developed for upscaling the matrix tortuosity and sorption coefficient in fractured rocks using indicator geostatistics and transition probability models postulated to incorporate a hierarchical distribution of the reactive mineral facies.

[4] Since the late 1990s, many interesting investigations about spatial-scale relationships of transport parameters in porous media have been conducted at various scales ranging from pore scale and column experiments to field tracer tests [e.g., *Rubin*, 1997; *Ginn*, 1999; *Xu et al.*, 1999; *Davis et al.*, 2004; *Dai and Samper*, 2006; *Dai et al.*, 2006; *Kwicklis et al.*, 2006; *Robinson et al.*, 2007]. Scale dependence has been found in various transport parameters such as diffusion coefficients [*Liu et al.*, 2007; *Zhou et al.*, 2007; *Dai et al.*, 2007a], geochemical reaction rates [*Lichtner*, 1993; *Meile and Tuncay*, 2006; *Li et al.*, 2007], sorption coefficients [*Liu et al.*, 2008; *Dai et al.*, 2009], and retardation factors [*Rajaram*, 1997; *Samper and Yang*, 2006; *Dai et al.*, 2009]. Using the spectral approach within the Lagrangian framework, *Rajaram* [1997] derived analytical expressions of effective retardation factors in temporal and spatial domains by assuming a spatial correlation between hydraulic conductivity and retardation factor. His research reveals that the values of retardation factor change with scales, and the effective retardation factor is approximately its arithmetic mean when the temporal and spatial scales are sufficiently large. Similar conclusions were reached by *Fernàndez-Garcia et al.* [2005] through a study on the effective retardation factor of heterogeneous porous media. More studies on the scaling of the retardation factors in porous media can be found by *Robin et al.* [1991], *Tompson* [1993], *Burr et al.* [1994], *Cvetkovic and Dagan* [1994], *Chao et al.* [2000], and *Andersson et al.* [2004].

[5] For fractured rocks, scaling effects of transport parameters have been studied using the continuous-time random walk and memory functions [e.g., *Berkowitz and Scher*, 1998; *Cvetkovic et al.*, 2004; *Frampton and Cvetkovic*, 2007], and the dual-porosity model with mass transfer coefficients [e.g., *Huang and Hu*, 2001; *Hu and Huang*, 2002; *Reimus et al.*, 2003]. Among conceptual and mathematical models developed for reactive transport modeling in fractured rocks, the dual porosity model is widely used [e.g., *Robinson*, 1994; *Reimus and Callahan*, 2007]. In the dual-porosity model, the primary pathway for groundwater flow is assumed to be through fractures, and the water in the saturated, matrix material is considered immobile. Solutes move between the matrix and the fractures via the processes of matrix diffusion and they may react with the matrix minerals (we assume that the surface area of fracture coating minerals is substantially smaller than that of matrix minerals accessible after diffusion occurs). Solute storage time in the matrix depends on the matrix volume and the sorption reaction rates between fractures and immobile minerals. The combination of matrix diffusion and matrix sorption processes retards field-scale solute transport relative to nonreactive, fracture-flow-only migration rates, resulting in breakthrough curves with long tails [*Robinson*, 1994].

[6] The governing equations of the dual-porosity model are given below for describing solute transport in fracture and matrix material, respectively [*Tang et al.*, 1981; *Sudicky and Frind*, 1982; *Reimus et al.*, 2003]:

[7] Fracture

$$R_f \frac{\partial C_f}{\partial t} + v_f \frac{\partial C_f}{\partial x} - D_f \frac{\partial^2 C_f}{\partial x^2} - \left. \frac{\phi D_m}{b\eta} \frac{\partial C_m}{\partial y} \right|_{y=b} = 0 \qquad (1a)$$

[8] Matrix

$$R_m \frac{\partial C_m}{\partial t} - D_m \frac{\partial^2 C_m}{\partial y^2} = 0, \qquad (1b)$$

where subscripts f and m denote the fracture and matrix domains, respectively; C is concentration (mg/L); v is flow velocity (cm/s); $D_m = D_0\tau$ is the matrix diffusion coefficient, which is the product of the free water diffusion coefficient (D_0) and the matrix tortuosity (τ); D_f is the dispersion coefficient in the fractures (cm^2/s); R_m is the retardation factor in the matrix, $R_m = 1 + (\rho/\phi)K_d$ for linear sorption reaction; R_f is the fracture retardation factor (assumed to be 1 here); ρ is the matrix bulk density (g/cm^3); ϕ is matrix porosity; K_d is the sorption coefficient (cm^3/g), which is the ratio of the sorbed concentration of a chemical species in the solid phase to its dissolved concentration in water; b is the fracture half aperture (cm); and η is porosity within the fractures. The x axis is defined in the direction of fracture flow, while y is normal to the flow direction, representing diffusive transport into the matrix material. Based on these governing equations, a mass transfer coefficient C_{MT} is defined as [*Reimus et al.*, 2003]

$$C_{MT} = \frac{\phi}{\eta b}\sqrt{R_m \tau D_0}. \qquad (2)$$

C_{MT} is a lumped parameter to describe the rate of a particular solute transferring between fracture and rock matrix. The mass transfer coefficient is a key variable for the proposed upscaling methods described in section 4.

[9] The scaling effect of the matrix sorption coefficients for a chemical species is closely related to the spatial variability of reactive mineral facies [e.g., *Zavarin et al.*, 2004; *Allen-King et al.*, 2006], because different spatial distributions of the reactive mineral facies determine different correlation lengths, composite means, and variances of tortuosity and sorption coefficient, which in turn result in different covariance functions for sorption coefficients. *Allen-King et al.* [1998] applied a sedimentary facies-based approach to characterize the heterogeneity and correlation of the perchloroethene (PCE) sorption coefficient at the Borden site. Their results show that the facies-based method is very useful for linking the sorption coefficient heterogeneity with the site sedimentary structures. At the Nevada Test Site, *Zavarin et al.* [2004] studied the heterogeneity of radionuclide sorption coefficients in volcanic rocks with different mineral facies. The covariance of uranium sorption coefficients, computed theoretically using surface complexation reaction equations, measured mineral contents, and assumed site exposure in vertical boreholes at that site fits an exponential function well (Figure 1) [*Stoller-Navarro Joint Venture*, 2009].

[10] Spatial distributions of reactive mineral facies in sediments are often composed of hierarchical structure,

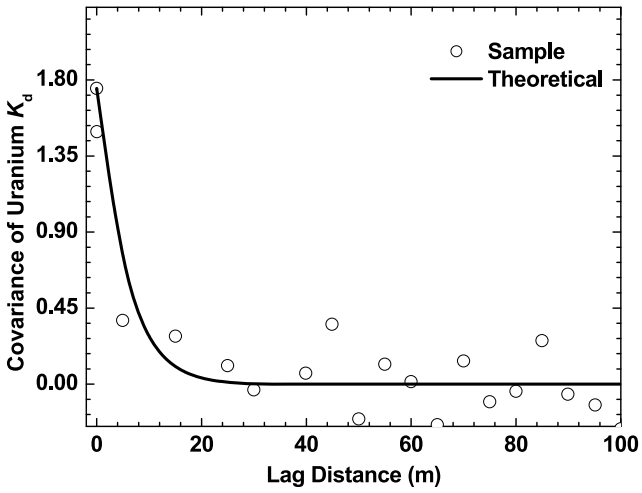

Figure 1. Covariance of uranium sorption coefficient (K_d) fits an exponential function well in the vertical direction (modified from *Stoller-Navarro Joint Venture* [2009]).

which can be decomposed into successively nested, interacting, physical subunits with multiple levels of tree-like structures of reactive mineral distributions [*Cushman*, 1990]. The hierarchical structures of mineral facies can be characterized using indicator geostatistics together with transition probability models [*Dai et al.*, 2004, 2005; *Ritzi et al.*, 2004]. Specifically, when a reactive mineral facies is made up of multiple reactive minerals that have very different mean sorption coefficients for a chemical species, the reactive mineral facies is characterized by a multimodal statistical distribution for the sorption coefficients. Because the transport parameters are spatially heterogeneous at various scales, one must characterize the spatial distributions of the mineral facies and the physical and chemical heterogeneities that control sorption processes.

[11] In the following sections a conceptual model is first developed for characterizing the reactive mineral facies with hierarchical structures. On the basis of the conceptual model, analytical expressions for upscaling the matrix tortuosity and sorption coefficients are then derived from the volume averaging of mass transfer coefficients between heterogeneous matrix and fracture. The upscaling equations provide effective transport parameters such as matrix tortuosity and sorption coefficient from the bench to field or modeling grid scales. Monte Carlo simulations are finally designed to verify the upscaling methods. In this study, only linear sorption reactions are considered between reactive minerals and dissolved uranium in water [e.g., *Davis et al.*, 2004]. We also assume that the linear sorption coefficients of uranium follow a lognormal distribution in each reactive mineral assemblage. The upscaling method is not limited to uranium, and can be easily extended to other contaminants and types of reactions.

2. Conceptual Model for Hierarchical Structure of Multimodal Reactive Mineral Facies

[12] Geochemical reactions in groundwater depend not only on aqueous-phase chemical species and physiochemical conditions (e.g., temperature, salinity, oxygen fugacity, pH, and Eh), but also on reactive mineral facies and their spatial distributions. In fractured rocks, reactive minerals adsorbing contaminants on their surfaces play a critical role in retarding contaminant migration rates. Because different reactive minerals have different sorption capacities, spatial variability of the reactive minerals significantly affects the sorption process and thus contaminant transport. From small to large scales, the reactive minerals constitute reactive mineral assemblages, which in turn form reactive mineral facies. As an analog to sedimentary facies with hierarchical architecture [*Scheibe and Freyberg*, 1995; *Dai et al.*, 2004], a hierarchical structure of mineral facies is constructed to analyze spatial distributions of reactive mineral facies in the matrix material and to upscale the matrix sorption coefficient in fractured rocks.

[13] Figure 2 illustrates the multiscale conceptual model developed based on a simplified synthesis of uranium transport in altered fractured volcanic rocks [*Stoller-Navarro Joint Venture*, 2009]. This conceptual model can be easily extended to other contaminants in other geological media. The volcanic rocks described here are pyroclastic rocks composed of ash flow tuffs and ashfall deposits of generally rhyolitic composition with some rhyolitic lava flows and basaltic rocks. The silica-rich ash flow and ashfall tuffs can be composed of more than 80% glass when originally deposited, with the remainder including original phenocrysts and lithic fragments. However, posteruption processes such as welding, devitrification, zeolitization, carbonatization, and argillization significantly alter the mineralogy and reactive transport properties of the volcanic rocks. Generally, the altered volcanic rocks display very consistent mineralogy that tends to change with type and intensity of alteration, i.e., a certain mineral association corresponds to a certain overlap of alteration types.

[14] As depicted in Figure 2, the distributions of reactive mineral facies are characterized in a three-tiered hierarchy with a population of uranium sorption coefficients at each hierarchical level. This hierarchy is an organized framework of sorption reactions between reactive minerals and dissolved uranium in water. However, the conceptual model and methods developed in this paper are not limited to the particular organization used for uranium sorption reaction and can be extended to be suitable to different reactions and different chemical species.

2.1. Reactive Minerals at Microform Scale

[15] Reactive minerals at the microform scale (10^{-6} to 10^{-2} m) refer to any minerals that are sensitive to one or a group of specified geochemical reactions. As shown in Figure 2a, the reactive minerals represent the lowest level of the hierarchical structure, equivalent to the scale of mineral grains in a rock thin section. In general, an individual mineral occurs at scales less than 1 cm in natural rocks. The smaller the mineral grain size, the larger the mineral surface area. Minerals with large surface areas usually have relatively large sorption coefficients [*Stumm and Morgan*, 1995]. For a given type of reactive mineral, the variation in uranium sorption coefficients is dependent not only on grain size and shape, but also on texture, crystal structure, variability of chemical composition of the minerals, and fluctuation in physical and chemical conditions under which the sorption reaction takes place [*Stumm and Morgan*, 1995]. Since pure reactive mineral separates are obtained from synthesis or the

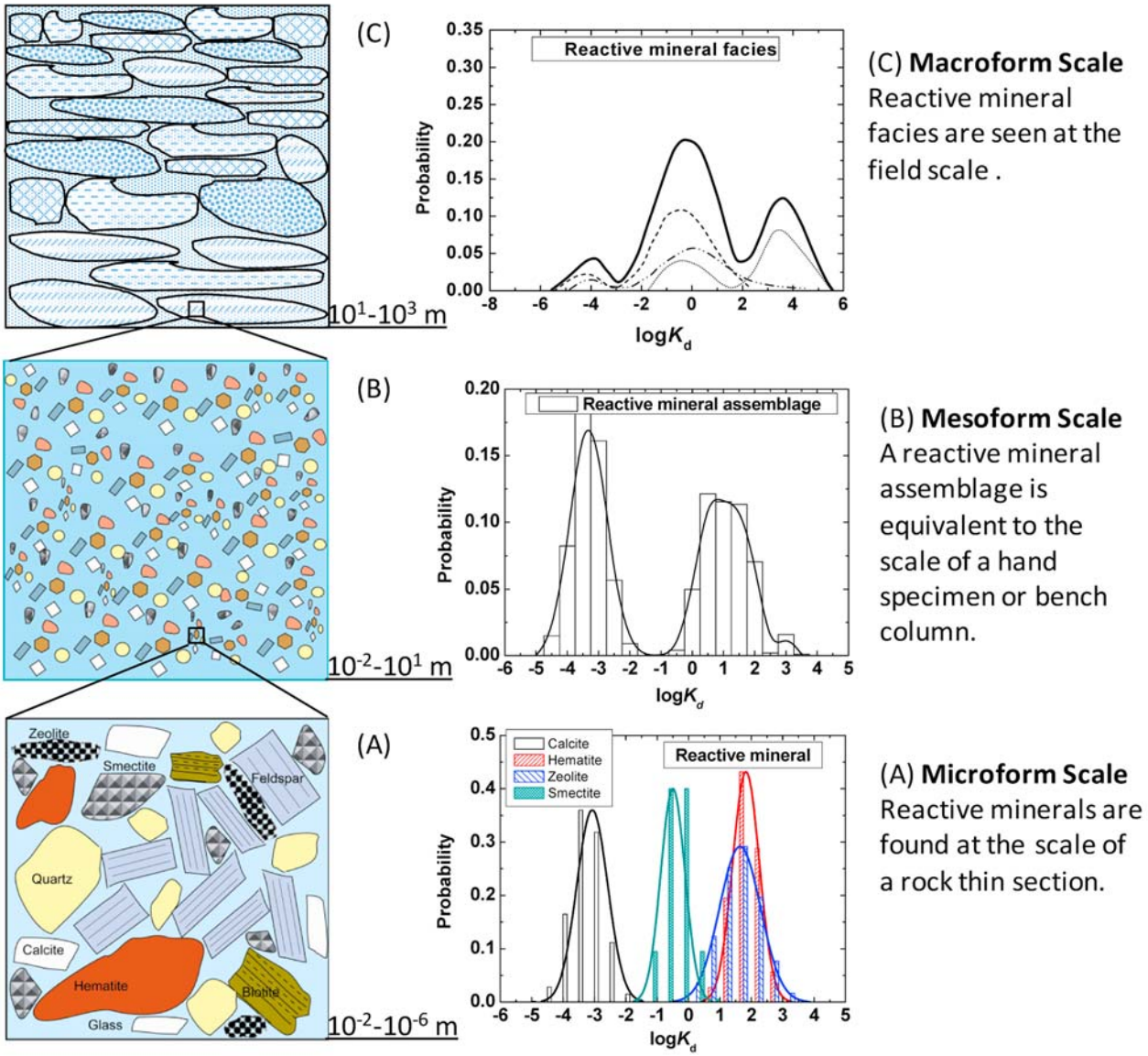

Figure 2. Hierarchical structure of reactive mineral facies. The distributions of uranium matrix sorption coefficients for reactive minerals are abstracted from *Zavarin et al.* [2004] and *Stoller-Navarro Joint Venture* [2009].

separation process, their sorption coefficients can be measured in tubes under controlled physiochemical conditions after the reactive mineral size and surface area are determined. Different reactive minerals usually have different sorption coefficients for uranium, as displayed by the four histograms shown in Figure 2a (data summarized from *Zavarin et al.* [2004] and *Stoller-Navarro Joint Venture* [2009]). For example, hematite has a higher uranium sorption coefficient than calcite because hematite has a larger reactive surface area per volume due to more reactive sites and smaller grain sizes.

[16] In altered volcanic rocks, the reactive minerals influencing mobility and fate of uranium include primary minerals, formed through crystallization during accumulation and eruption of magma, and secondary minerals, formed by alteration and weathering after eruption. The primary reactive mineral considered in this study is hematite and the secondary reactive minerals are smectite, zeolite, Fe-oxides, and calcite. Figure 2a shows four reactive minerals: hematite, zeolite, smectite, and calcite, of which hematite includes all kinds of Fe-oxides from alterations.

[17] The primary volcanic glass, which comprises up to 80% weight of the volcanic rocks, is not considered as a reactive mineral for uranium sorption [*Stoller-Navarro Joint Venture*, 2009]. The microcrystalline quartz and feldspar from devitrification of the glass and other primary minerals (e.g., feldspar, hornblende, pyroxene, and olivine) are not considered as reactive minerals because they have extremely low sorption coefficients for uranium. Although these nonreactive minerals have little impact on uranium sorption reactions, the nonreactive minerals make up a large volumetric proportion of the rocks. Therefore, the spatial dis-

Table 1. Reactive Mineral Assemblages That Are Composed of Reactive Minerals and Nonreactive Minerals for Uranium Sorption in Altered Volcanic Rocks[a]

RMA	Typical Lithology	Major Alteration	RM	NRM	Identification Criteria
Zeolite RMA (ZRMA)	Bedded tuff, nonwelded tuff	Zeolitization Argillization	Ze, Smt	Glass, Qtz, Fl	>20% Ze Ze > clay <10% glass
Vitric mafic-rich RMA (VMRRMA)	Nonwelded ash flow tuff, bedded/ashfall tuff	Argillization Carbonatization Zeolitization	Smt, Cc, Ze, Fe-oxides	Glass, Fl, Bi, Hb, Hm, Mt, Px	>30% glass <10% clay <8% Ze >1.5% Bi + Hb
Vitric mafic-poor RMA (VMPRMA)	Nonwelded ash flow tuff, bedded/ashfall tuff	Argillization Zeolitization Carbonatization	Smt, Ze, Cc	Glass, Fl, Qtz	>30% glass <10% clay <20% Ze <1.5% Bi + Hb
Devitrified mafic-rich RMA (DMRRMA)	Welded ash flow tuff	Devitrification Argillization Carbonatization Zeolitization	Smt, Ze, Cc, Fe-oxides	Glass, Fl Qtz, Bi, Hm Mt, Hb, Px	<20% glass >60% Qtz + Fl <17% Ze >1.5% Bi + Hb
Devitrified mafic-poor RMA (DMPRMA)	Welded ash flow tuff	Devitrification Zeolitization Carbonatization	Smt, Ze, Cc, Fe-oxides	Glass, Fl, Qtz	<20% glass >60% Qtz + Fl <15% Ze <1.5% Bi + Hb
Primary magmatic mineral assemblage (PMMA)	Ash flow tuff Bedded tuff Ashfall tuff	No alterations	Magmatic hematite	Glass, Fl, Qtz, Bi, Hm, Mt, Hb, Px	No alteration minerals (clays, Ze, Smt, Cc, and secondary Fe-oxides)

[a]RM, reactive minerals; NRM, Nonreactive minerals; Qtz, quartz; Fl, feldspar; Bi, biotite; Hb, hornblende; Mt, magnetite; Px, pyroxene; Hm, hematite; Ze, zeolite; Smt, smectite; Cc, calcite. Modified from *Wolfsberg et al.* [2002].

tributions of the nonreactive minerals can result in heterogeneous patterns of the reactive minerals and in turn affect the statistical properties (e.g., proportion and correlation length) of the reactive minerals.

2.2. Reactive Mineral Assemblages at the Mesoform Scale

[18] In practice, when one cannot obtain purely separated minerals for column experiments to measure sorption coefficients, one must use reactive mineral assemblage to do column experiments. A reactive mineral assemblage at the mesoform scale (10^{-2} to 10^{1} m) is an association of coexisting nonreactive and reactive minerals for one or a group of specified geochemical reactions. The mesoform scale ranges from a hand specimen or experimental column to a small rock outcrop (Figure 2b). Usually, a certain mineral assemblage corresponds to a certain geochemical process by which it was formed. For example, zeolitization results in zeolite, with minor amounts of smectite and hematite. On the other hand, different types of alterations may overlap to different degrees in space, resulting in a close spatial association of several different reactive minerals in the altered volcanic rocks. Different reactive mineral assemblages can be composed of the same nonreactive and reactive minerals, but with very different volumetric proportions of each reactive mineral. Therefore, different reactive mineral assemblages have different capacities for controlling one or a group of specified geochemical reactions. Besides the reactive mineral assemblages (RMA) in the altered volcanic rocks, there can be one or several nonreactive mineral assemblages (NRMA). Table 1 summarizes the RMAs that are composed of reactive minerals and nonreactive minerals for uranium sorption in altered volcanic rocks, in which five RMAs have been identified and one NRMA is distinguished as a part of the primary magmatic mineral assemblage (PMMA) [*Stoller-Navarro Joint Venture*, 2009].

[19] Owing to different statistical distributions of the uranium sorption coefficients among different reactive minerals (Figure 2a), the different RMA may have different statistical distributions of uranium sorption coefficients. If the mean difference of uranium sorption coefficients between different reactive minerals is large enough, the RMA composed of the reactive minerals will have a multimodal statistical distribution for the uranium sorption coefficients (Figure 2b). If an RMA consists of only one kind of reactive mineral or several kinds of reactive minerals with similar mean sorption coefficients, its sorption coefficient will have a single mode (close to the mean of the reactive minerals) with a variance larger than that at the microform scale.

[20] NRMAs have negligible uranium sorption coefficients and do not directly influence sorption capacities of altered volcanic rocks. However, the spatial distributions of NRMAs among RMAs do affect the spatial heterogeneity of RMA distributions, and the latter cause the heterogeneity of the sorption coefficients at the larger scale, i.e., in reactive mineral facies.

[21] Figure 2c displays the reactive mineral facies at the macroform scale (10^{1} to 10^{3} m), the top hierarchical level. The macroform scale is equivalent to the field scale, at which the field reactive transport modeling, contaminant remediation, and risk assessment are actually conducted. A reactive mineral facies is a body of rock that is characterized by a few reactive and nonreactive mineral assemblages for one or a group of specified geochemical reactions. Volcanic eruptions in a specified area during a specified period are discontinuous and episodic, which results in multiple volcanic sequences in the area, each of which may have different types of rocks and alterations. Due to temporal and

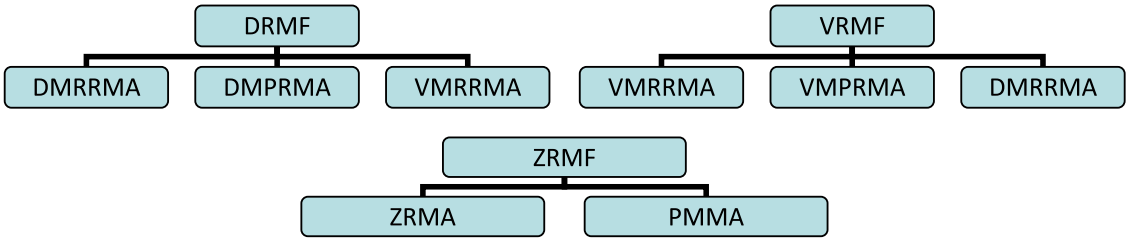

Figure 3. Sketch showing the composition of three reactive mineral facies based on reactive mineral assemblages as defined in Table 1.

spatial variability of alteration and devitrification of the volcanic rocks within a specified eruption sequence, the spatial distributions of reactive mineral assemblages are heterogeneous within the volcanic formations. The concept of reactive mineral facies is thus introduced as an association of the reactive mineral assemblages to describe the alignment patterns of the assemblages.

[22] Three types of reactive mineral facies are summarized in this study on the basis of types and intensity of distinct alteration and of different degrees to which the reactive mineral facies influence uranium sorption in the matrix [*Wolfsberg et al.*, 2002]. They are devitrified reactive mineral facies (DRMF), vitric reactive mineral facies (VRMF), and zoelitization reactive mineral facies (ZRMF). Figure 3 illustrates the relationship between each of the reactive mineral facies and the reactive mineral assemblages as defined in Table 1. For example, the DRMF is composed of devitrified mafic-rich (combined calcium, magnesium, and iron mineral proportions >1.5%) and mafic-poor (same mineral proportions <1.5%) reactive mineral assemblages (DMRRMA and DMPRMA) and vitric mafic-rich reactive mineral assemblage (VMRRMA). The multimodal reactive mineral assemblages (Figure 2b) result in the multimodal reactive mineral facies (Figure 2c).

[23] This conceptual model of the hierarchical structure of the reactive mineral facies provides a basis for upscaling the sorption coefficient. After all appropriate reactive mineral facies are identified and their hierarchical structure is established, a multimodal covariance function is developed for upscaling sorption coefficient using indicator geostatistics and a transition probability model [e.g., *Journel*, 1983; *Ritzi*, 2000; *Ye and Khaleel*, 2008] to describe distribution patterns of reactive minerals and reactive mineral assemblages.

3. Spatial Statistics of Multimodal Tortuosity and Retardation Factor

[24] Although the conceptual model above contains the three hierarchical levels of the sorption coefficient, for the purpose of demonstration, the upscaling equations developed below are only for two levels, i.e., from the reactive mineral assemblages to the reactive mineral facies. These equations can be easily extended to any number of hierarchical levels as suggested by *Dai et al.* [2005]. Consider a domain Ω filled with N reactive mineral assemblages of mutually exclusive occurrences. Denoting the volumetric proportion of the kth reactive mineral assemblage as p_k, then $\sum_{k=1}^{N} p_k = 1$. Let $X(\mathbf{x})$ be a multimodal spatial random variable for either log tortuosity ($\ln\tau$) or log retardation factor ($\ln R_m$). It can be expressed as

$$X(\mathbf{x}) = \sum_{k=1}^{N} I_k(\mathbf{x}) X_k(\mathbf{x}), \tag{3}$$

where $X_k(\mathbf{x})$, $k = \overline{1,N}$ represents the property $X(\mathbf{x})$ of different reactive mineral assemblages k at location $\mathbf{x}$, and $I_k(\mathbf{x})$, $k = \overline{1,N}$ is an indicator of spatial random variable defined within the domain Ω as

$$I_k(\mathbf{x}) = \begin{cases} 1, \text{if reactive mineral assemblage } k \text{ occurs at location } \mathbf{x} \\ 0, \text{otherwise} \end{cases}. \tag{4}$$

Following *Ritzi et al.* [2004] and *Huang and Dai* [2008], the composite mean M_X and composite variance σ_X^2 of the property are calculated via

$$M_X = \sum_{k=1}^{N} p_k m_k, \tag{5}$$

$$\sigma_X^2 = \sum_{k=1}^{N} p_k \sigma_k^2 + \frac{1}{2} \sum_{k=1}^{N} \sum_{i=1}^{N} p_k p_i (m_k - m_i)^2, \tag{6}$$

where m_k and σ_k^2 are the mean and variance of $X_k(\mathbf{x})$ for the reactive mineral assemblage k, respectively.

[25] Taking two locations, $\mathbf{x}$ and $\boldsymbol{\chi}$, separated by a distance vector h_φ in the φ direction, the transition probability $t_{ki}(\mathbf{x}, \boldsymbol{\chi})$ is defined as the conditional probability for the reactive mineral assemblage i occurring at location $\boldsymbol{\chi}$, given the other reactive mineral facies k occurs at location $\mathbf{x}$:

$$\begin{aligned} t_{ki}(\mathbf{x}, \boldsymbol{\chi}) &= \Pr\{I_i(\boldsymbol{\chi}) = 1 | I_k(\mathbf{x}) = 1\} \\ &= \Pr\{I_i(\boldsymbol{\chi}) = 1 \text{ and } I_k(\mathbf{x}) = 1\} / \Pr\{I_i(\boldsymbol{\chi}) = 1\}. \end{aligned} \tag{7}$$

Assuming that both covariance function (Figure 1) and transition probability are exponential [*Dai et al.*, 2007b], and that the cross-covariances are negligible [*Lu and Zhang*, 2002; *Dai et al.*, 2004], the composite covariance function

Table 2. Statistical Parameters for a Synthetic Field-Scale Heterogeneous Matrix System

Assemblages	p_k	Parameter	m_k	σ_k^2	M_k^G	λ_k (m)	$\lambda_{\psi,k}$ (m)
		τ	−3.2	0.22	0.041	10	6.67
F1	0.60	R_m	3.1	0.30	22.20	12	7.50
		K_d (cm^3/g)	0.53	–	1.70	–	–
		τ	−2.6	0.20	0.074	6	4.62
F2	0.15	R_m	4.8	0.12	121.51	8	5.71
		K_d (cm^3/g)	2.27	–	9.64	–	–
		τ	−4.5	0.15	0.011	7	5.19
F3	0.25	R_m	4.6	0.10	99.48	9	6.21
		K_d (cm^3/g)	2.06	–	7.88	–	–
σ_τ^2	$\sigma_{R_m}^2$	τ^G	R_m^G	$\tilde{\tau}$	$\tilde{D}$ (m^2/s)	$\tilde{R}_m$	$\tilde{K}_d$ (cm^3/g)
0.621	0.822	0.032	41.68	0.0374	2.48×10^{-11}	49.31	3.87
ρ (g/cm^3)	ϕ	D_0 (m^2/s)	K_d^G (cm^3/g)	L (m)	λ_I (m)	λ_τ (m)	λ_{Rm} (m)
2.50	0.20	6.64×10^{-10}	3.25	1000	20	15.99	17.15

for tortuosity ($\ln\tau$) or the retardation factor ($\ln R_m$) is expressed as [*Dai et al.*, 2004]

$$C_X(h_\varphi) = \sum_{k=1}^{N} p_k^2\sigma_k^2 e^{-\frac{h_\phi}{\lambda_k}} + \sum_{k=1}^{N} p_k(1-p_k)\sigma_k^2 e^{-\frac{h_\phi}{\lambda_\psi}} + \frac{1}{2}\sum_{k=1}^{N}\sum_{i=1}^{N}(m_k - m_i)^2 p_k p_i e^{-\frac{h_\phi}{\lambda_I}}, \quad (8)$$

where $\lambda_\psi = \lambda_k\lambda_I/(\lambda_k + \lambda_I)$, λ_k and λ_I are the integral scale of the reactive mineral assemblage k and the indicator correlation length, respectively. For a set of given parameters (Table 2), the composite covariance of the retardation factor and the covariance for each reactive mineral assemblage are shown in Figure 4, which illustrates the relationship among the composite covariance and the individual reactive mineral assemblage covariance.

[26] Table 2 lists synthetic parameters that are used to illustrate the relationship among variables applied for upscaling (Figures 4–8 and 14) and Monte Carlo simulations (Figures 9, 11, and 13). The ranges of synthetic parameters are summaries based on representative column experiments reported for altered volcanic tuffs [*Wolfsberg et al.*, 2002; *Zavarin et al.*, 2004; *Stoller-Navarro Joint Venture*, 2009]. In Table 2, the statistical values of composite parameters stand for those of a reactive mineral facies, DRMF, made up of three reactive mineral assemblages F1, F2, and F3, which approximately represent DMRRMA, DMPRMA, and VMRRMA, respectively (Table 1 and Figure 3).

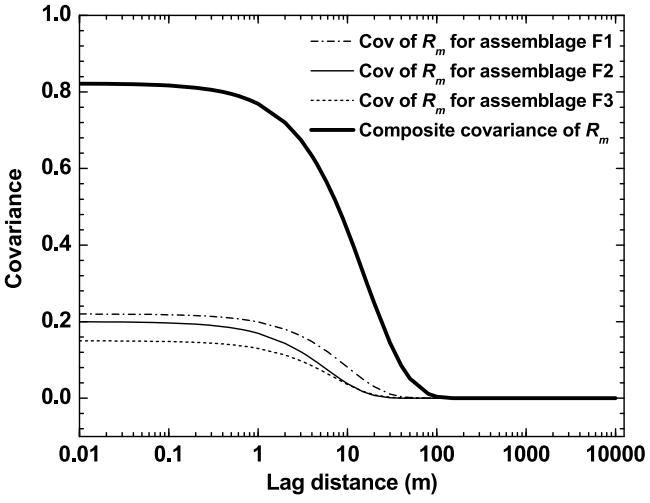

Figure 4. Covariances of retardation factors of reactive mineral assemblage F1, F2, and F3 (the statistical parameters are from Table 2). The global or composite covariance is calculated according to equation (8).

4. Upscaling Retardation Factors and Sorption Coefficients in a Multimodal Matrix

[27] In fractured rocks the mass transfer coefficient defined in equation (2) is a lumped parameter that expresses the transfer rate of a particular solute between fracture and matrix. One approach to obtain the effective mass transfer

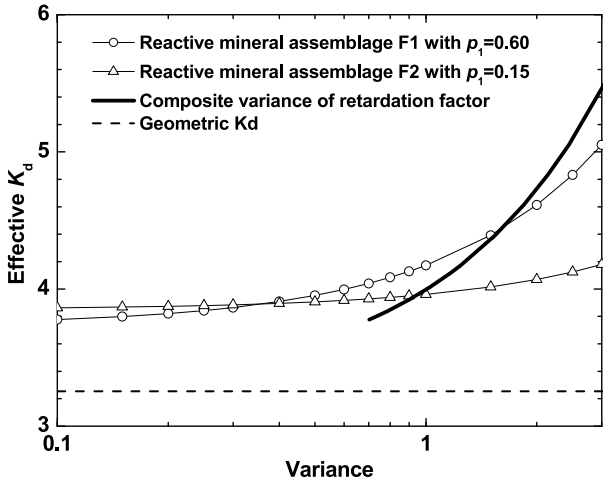

Figure 5. Effective sorption coefficient increases with the composite variance of retardation factor for reactive mineral facies, and variances of retardation factor for reactive mineral assemblages F1 and F2. The reactive mineral assemblage F1 (0.6) has larger volume proportion than F2 (0.15). Thus, an increase in variance of the retardation factor for reactive mineral assemblage F1 has more significant influences on effective K_d than that of reactive mineral assemblage F2. For comparison, the geometric mean of the sorption coefficient is about 3.25 cm^3/g; the composite variance of retardation factor used in Monte Carlo simulation is 0.822 (Table 2).

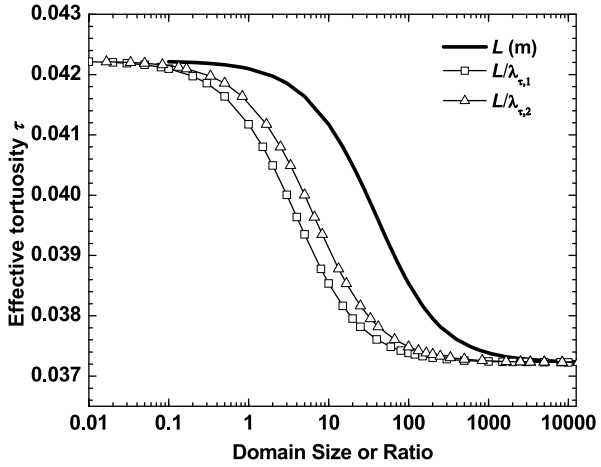

Figure 6. Effective tortuosity decreases with L/λ, the ratios of domain size to the integral scales of reactive mineral assemblages F1 and F2, respectively, and decreases with the domain size (L), in which the integral scale of reactive mineral assemblages remain unchanged. The geometric mean of the tortuosity is about 0.032.

coefficient at the field scale (equivalent to reactive mineral facies) is to upscale the mass transfer coefficient measured at smaller scale (column experiment on reactive minerals or tracer tests on reactive mineral assemblages) by simple volume averaging (simplified from *Rubin* [2003, p. 163]):

$$\tilde{C}_{\mathrm{MT}} = \frac{\tilde{\phi}}{\eta \tilde{b}} \sqrt{D_0 \tilde{\tau} \tilde{R}_m} = \frac{1}{L} \int_L \frac{\phi \sqrt{D_0 \tau R_m}}{\eta b} dx, \tag{9}$$

where $\tilde{C}_{\mathrm{MT}}$ is the effective mass transfer coefficient; $\tilde{\phi}$ is the effective matrix porosity; $\tilde{b}$ is the effective half aperture of the fracture; $\tilde{\tau}$ is the effective matrix tortuosity; $\tilde{R}_m$ is the effective retardation factor for matrix; x is the spatial coordinate along the fracture; and L is the length of a1-D domain which is a simplified replace of volume due to the constant matrix spacing and thickness. While a simple volume average does not always accurately represent an upscaled effective property, we employ this approach here because (1) there is an expectation that the arithmetic average consistently represents the effective mass transfer coefficient based on previous results on the retardation factor [*Rajaram*, 1997; *Dai et al.*, 2009] and (2) the volume-averaged mass transfer coefficient leads to good agreement with Monte Carlo simulation results presented in a later section.

[28] We assume the tortuosity and retardation factor as second-order stationary random variables, and express them as in equation (9) (the fracture porosity η is assumed to be 1, i.e., open fractures). In the most general case, $\tilde{R}_m$, $\tilde{\tau}$, $\tilde{\phi}$, and $\tilde{b}$ would all be random variables in equation (9), and they may be correlated with each other to varying degrees for a given mineral facie. In this paper, we assume effective values of matrix porosity and fracture aperture ($\tilde{\phi}$ and $\tilde{b}$) can be estimated independently from measurements at smaller scales, and we focus only on the dependence of the mass transfer coefficient on $\tilde{R}_m$ and $\tilde{\tau}$. Furthermore, even though the sorption coefficient K_d is technically the fundamental parameter describing contaminant-rock interactions, we consider $\tilde{R}_m$ (which contains the added influence of matrix porosity) to be the primary random variable describing contaminant-rock interactions here. The scale dependence of contaminant transport on K_d is then inferred from the dependence of K_d on $\tilde{R}_m$.

[29] $\tilde{R}_m$ and $\tilde{\tau}$ are assumed second-order stationary random variables, expressed as

$$\ln \tau = Z(x) \text{ and } Z(x) = M_Z + Z'(x) \tag{10a}$$

$$\ln R_m = Y(x) \text{ and } Y(x) = M_Y + Y'(x). \tag{10b}$$

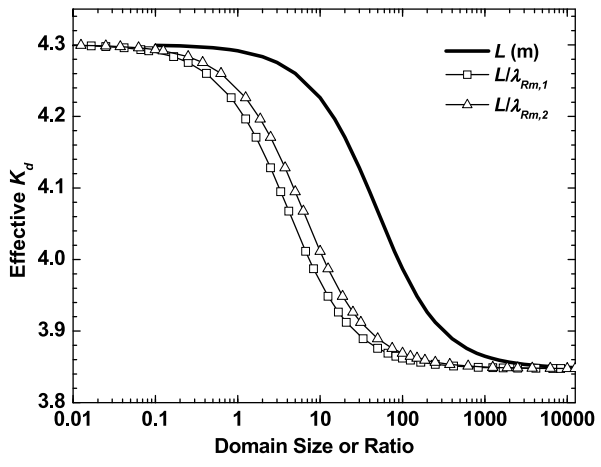

Figure 7. Effective sorption coefficient decreases with L/λ, the ratios of domain size to the integral scales of reactive mineral assemblages F1 and F2, respectively, and decreases with the domain size (L), in which the integral scale of reactive mineral assemblages is unchanged. The geometric mean of the sorption coefficient is about 3.25 cm^3/g.

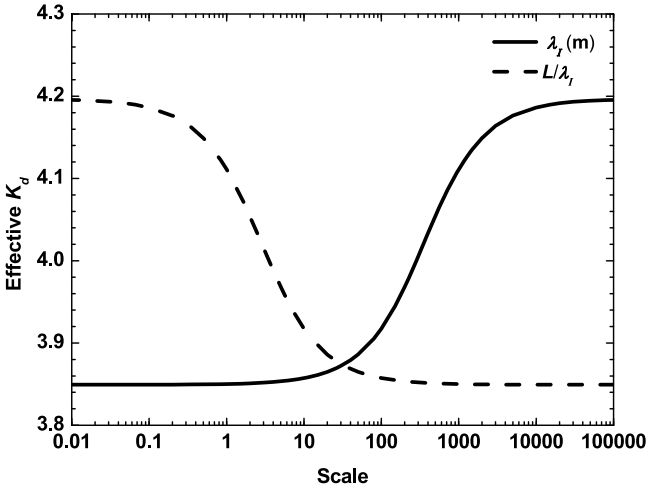

Figure 8. Effective sorption coefficient increases with correlation length of indicator variable and decreases with the ratio of domain size to correlation length of indicator variable, in which the domain size keep constant, L = 1000 m. For comparison, the geometric mean of the sorption coefficient is about 3.25 cm^3/g.

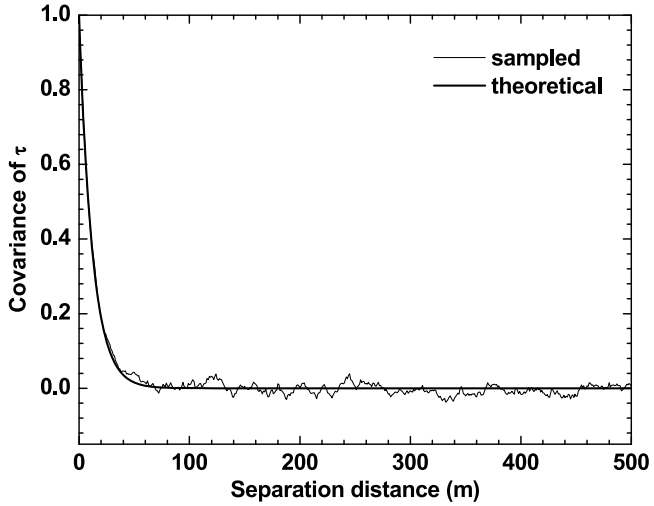

Figure 9. Comparison of the sampled and the theoretical covariance of tortuosity for reactive mineral facies 2.

Rearranging equation (9) and substituting equation (10) into the rearranged (9) leads to

$$\tilde{\tau}\tilde{R}_m = \left(\frac{1}{L}\int_L e^{\frac{1}{2}[Y(x)+Z(x)]}dx\right)^2 \tag{11}$$

$$\tilde{\tau}\tilde{R}_m = \frac{R_m^G \tau^G}{L^2}\left(\int_L\int_L e^{\frac{1}{2}(Y'(x)+Y'(y)+Z'(x)+Z'(y))}dxdy\right), \tag{12}$$

where $R_m^G = e^{M_Y}$ and $\tau^G = e^{M_Z}$ are the geometric means of the measurement-scale retardation factor and tortuosity and y is also a 1-D spatial variable similar to x. Applying the Taylor series expansion to the exponential term in equation (12), assuming that the variance of $Y(x)$ and $Z(x)$ is smaller than 1, and taking expectation of both sides of the equation, we have

$$\langle\tilde{\tau}\tilde{R}_m\rangle = R_m^G\tau^G\left\{1+\frac{\sigma_Y^2+\sigma_Z^2}{4}+\frac{1}{4L^2}\left[\int_L\int_L (C_Y(x,y)+C_Z(x,y) + \omega_{YZ}(x,y))dxdy\right]\right\}, \tag{13}$$

where the operator $\langle\ \rangle$ denotes expectation, σ_Y^2 and σ_Z^2, defined in equation (6), are composite variances of log retardation factor and log tortuosity, $C_Y(x,y) = \langle Y'(x)Y'(y)\rangle$ and $C_Z(x,y) = \langle Z'(x)Z'(y)\rangle$ are the covariance of Y and Z defined in equation (8), and $\omega_{YZ}(x, y) = \langle Y'(x)Z'(x) + Y'(x)Z'(y) + Y'(y)Z'(y) + Y'(y)Z'(x)\rangle$ is the sum of one-point and two-point cross-covariances between the retardation factor and the tortuosity. Assuming that the random field of the retardation factor is independent of that of the tortuosity, $\omega_{YZ}(x, y) = 0$. This assumption is often not valid in real systems because matrix tortuosity may be positively correlated with matrix porosity (e.g., Archie's law [*Archie*, 1947]), and the matrix retardation factor, in turn, is inversely proportional to matrix porosity (via the definition $R_m = 1 + (\rho/\phi)K_d$). However, we make an assumption of zero cross-covariance here because our example problem (described later) involves only a very small cross-covariance between the matrix retardation factor and matrix tortuosity, and also because this assumption greatly simplifies the subsequent derivations that serve to illustrate the theoretical basis for a heterogeneity-based-scale dependence. Although the case of nonzero cross-covariance can be handled easily within the theoretical framework developed below, assumption of zero cross-covariance allows for more tractable derivations and explanations.

[30] For a nonreactive solute or tracer (such as bromine), $R_m = 1$, $\sigma_Y^2 = 0$, and $C_Y(x, y) = 0$. Substituting equation (8) into equation (13) gives

$$\langle\tilde{\tau}\rangle = \tau^G\left\{1+\frac{\sigma_Z^2}{4}+\frac{1}{2L^2}\left[\sum_{k=1}^N p_k^2\sigma_k^2\lambda_k^2\left(\frac{L}{\lambda_k}-1+e^{-\frac{L}{\lambda_k}}\right) + \sum_{k=1}^N p_k(1-p_k)\sigma_k^2\lambda_\psi^2\left(\frac{L}{\lambda_\psi}-1+e^{-\frac{L}{\lambda_\psi}}\right) + \frac{1}{2}\sum_{k=1}^N\sum_{i=1}^N (m_k-m_i)^2 p_k p_i \lambda_I^2\left(\frac{L}{\lambda_I}-1+e^{-\frac{L}{\lambda_I}}\right)\right]\right\}. \tag{14}$$

This is the upscaling equation of the tortuosity for a multimodal matrix, which has a similar structure as the upscaling equation of the matrix diffusion coefficient (D_m) by *Dai et al.* [2007a]. When $N = 1$, equation (14) is reduced to the expression for a unimodal matrix, the same as equation (10) of *Dai et al.* [2009].

[31] Substituting the covariance expression for the $Y(x)$ and $Z(x)$ from equation (8) into equation (13) and dividing the effective tortuosity $\langle\tilde{\tau}\rangle$ from both sides of the equation, we get the upscaling expression for the retardation factor as

$$\langle\tilde{R}_m\rangle = R_m^G\left[1+\frac{\tau^G}{\langle\tilde{\tau}\rangle}\left(\frac{\sigma_Y^2}{4}+\frac{G}{2L^2}\right)\right], \tag{15}$$

where

$$G = \sum_{k=1}^N p_k^2\sigma_{Y,k}^2\lambda_k^2\left(\frac{L}{\lambda_k}-1+e^{-\frac{L}{\lambda_k}}\right) + \sum_{k=1}^N p_k(1-p_k)\sigma_{Y,k}^2\lambda_\psi^2\left(\frac{L}{\lambda_\psi}-1+e^{-\frac{L}{\lambda_\psi}}\right) + \frac{1}{2}\sum_{k=1}^N\sum_{i=1}^N p_k p_i\left(m_{Y,k}-m_{Y,i}\right)^2\lambda_I^2\left(\frac{L}{\lambda_I}-1+e^{-\frac{L}{\lambda_I}}\right). \tag{16}$$

Because $\tilde{K}_d = (\tilde{R}_m - 1)\tilde{\phi}/\rho$, the effective sorption coefficient for the multimodal matrix is obtained as

$$\langle\tilde{K}_d\rangle = \frac{R_m^G\tilde{\phi}}{\rho}\left\{\left[1+\frac{\tau^G}{\langle\tilde{\tau}\rangle}\left(\frac{\sigma_Y^2}{4}+\frac{G}{2L^2}\right)\right]-\frac{1}{R_m^G}\right\}. \tag{17}$$

When $N = 1$, equation (16) becomes

$$G = \sigma_Y^2\lambda_Y^2\left(\frac{L}{\lambda_Y}-1+e^{-\frac{L}{\lambda_Y}}\right). \tag{18}$$

Then, equations (15) and (17) are reduced to equations (19) and (20),

$$\langle \tilde{R}_m \rangle = R_m^G \left\{ 1 + \frac{\sigma_Y^2 \tau^G}{4\langle \tilde{\tau} \rangle} \left[1 + \frac{2\lambda_Y^2}{L^2} \left(\frac{L}{\lambda_Y} - 1 + e^{-\frac{L}{\lambda_Y}} \right) \right] \right\} \quad (19)$$

$$\langle \tilde{K}_d \rangle = \frac{R_m^G \tilde{\phi}}{\rho} \left\{ 1 + \frac{\sigma_Y^2 \tau^G}{4\langle \tilde{\tau} \rangle} \left[1 + \frac{2\lambda_Y^2}{L^2} \left(\frac{L}{\lambda_Y} - 1 + e^{-\frac{L}{\lambda_Y}} \right) \right] - \frac{1}{R_m^G} \right\}, \quad (20)$$

the exact expressions for unimodal matrix, i.e., equations (11) and (13) by *Dai et al.* [2009].

[32] When $L \to \infty$ or $\lambda_Y \to 0$, the random field of retardation factor is not correlated, and the effective sorption coefficient is

$$\langle \tilde{K}_d \rangle = \frac{R_m^G \tilde{\phi}}{\rho} \left(1 + \frac{\sigma_Y^2 \tau^G}{4\langle \tilde{\tau} \rangle} - \frac{1}{R_m^G} \right). \quad (21)$$

When L is sufficiently small or λ_k/L, λ_ψ/L, and λ_I/L are all sufficiently large, the correlation length is much larger than the domain size, and the effective sorption coefficient is

$$\langle \tilde{K}_d \rangle = \frac{R_m^G \tilde{\phi}}{\rho} \left(1 + \frac{\sigma_Y^2 \tau^G}{2\langle \tilde{\tau} \rangle} - \frac{1}{R_m^G} \right). \quad (22)$$

Equations (19) and (20) imply that if the composite variance of the retardation factor is zero (the matrix being homogeneous), the effective retardation factor and effective sorption coefficient are equal to their mean, respectively. This reveals that the scale dependence of the reactive transport parameter originates from medium heterogeneity. Figure 5 demonstrates that the effective sorption coefficient increases with the composite variance of the retardation factor of the reactive mineral facies and increases with the individual variance of the retardation factor in the reactive mineral assemblage F1 and F2. Furthermore, the variance of the reactive mineral assemblage F1 has a more significant influence on the effective transport parameters than that of F2 because F1 has a larger volumetric proportion (0.6) than F2 (0.15). Figure 5 also indicates that the effective sorption coefficients are always greater than the geometric mean of the sorption coefficients (3.25 cm^3/g). Note that the upscaling equations of the effective sorption coefficients are derived upon the linear perturbation assumption of the variance less than unity.

[33] By using the data listed in Table 2, the effective transport parameters are plotted with domain size (Figures 6 and 7) and integral scales of the reactive mineral assemblages (Figure 8). Figure 6 displays that the effective tortuosity decreases with the domain size (L) and with the ratios (L/λ) of the domain size to the integral scale of the reactive mineral assemblages F1 and F2 (for the latter, the integral scales are constants). This is also the case for the effective sorption coefficient (Figure 7). The same amount of decrease in the effective sorption coefficients requires almost the same amount of increase in the (L/λ) ratios for the reactive mineral assemblages F1 and F2. Figure 8 indicates that an increase in the integral scale of the indicator variables increases the effective sorption coefficients, and that the later decrease with increase in the ratio of domain size to the integral scale of the indicator variable. When the integral scale of the indicator variables is relatively small (i.e., less than about 30 m), the effective sorption coefficients are close to the lower limit; when the integral scale of indicator variable is very large, the effective sorption coefficients are close to the upper limit. The lower and upper limits correspond to values determined by equations (21) and (22). In general, the values of the effective reactive transport parameters are always larger than the geometric mean and increase with the correlation length and decrease with the domain size.

5. Verification of Upscaling Equations With Monte Carlo Simulations

[34] The developed upscaling equations for the matrix sorption coefficient are verified using Monte Carlo (MC) simulations. Multiple realizations of random fields for tortuosity and the retardation factor at mesoform scales are first generated for the MC simulations. Flow and transport simulations are conducted for each realization using the generalized double porosity model (GDPM) [*Zyvoloski et al.*, 2008]. Based on the statistics of the random fields listed in Table 2, the upscaled tortuosity and sorption coefficient are estimated for solving the flow and transport using the governing equations (1a) and (1b). The breakthrough curve of concentration computed from the upscaled parameters is compared with that of MC results to verify the developed upscaling method.

[35] The three reactive mineral assemblages considered in this study are DMRRMA, DMPRMA, and VMRRMA (see Table 1 and Figure 3). The spatial distributions of the three reactive mineral assemblages are simulated with Markovian indicator simulator T-PROGS [*Carle*, 1999; *Dai et al.*, 2007b]. Ten thousand indicator fields are generated for the tortuosity and retardation factor. Because the spatial distributions of the tortuosity and retardation factor are different in these three reactive mineral assemblages, each reactive mineral assemblage is associated with 10,000 Gaussian random fields of the two random variables (log tortuosity and log retardation factor) created with Karhunen-Loeve method [*Zhang and Lu*, 2004], respectively. Then the tortuosity random fields are used to generate the random fields of matrix diffusion coefficient through $D_m = D_0 \tau_m$; the random fields of the retardation factor are converted to the matrix sorption coefficient fields by $K_d = \phi/\rho(R_m - 1)$. Quality of the generated random fields is examined by comparing the covariance calculated from the generated realizations with the analytical exponential covariance models. An example is plotted in Figure 9 for the tortuosity of the reactive mineral assemblage 2. The sampled covariance agrees well with the analytical one. Similar investigations are conducted for the generated indicator random fields by comparing sampled and theoretical transition probability matrix. The comparisons show that the specified means, variances, mean lengths, and volumetric proportions are honored in the realizations.

[36] The dual porosity model for flow and transport in fractured rocks (equation (1)) is solved within a numerical simulator Finite Element Heat and Mass (FEHM) [*Zyvoloski et al.*, 2008]. In our case, the 2-D GDPM numerical model has a length of 1000 m with a fracture spacing of 2 m and aperture of 0.002 m (Figure 10). The fracture is discretized into 1000 uniform elements of 1 m, resulting in 1001 fracture nodes. Perpendicular to each fracture node, the matrix is

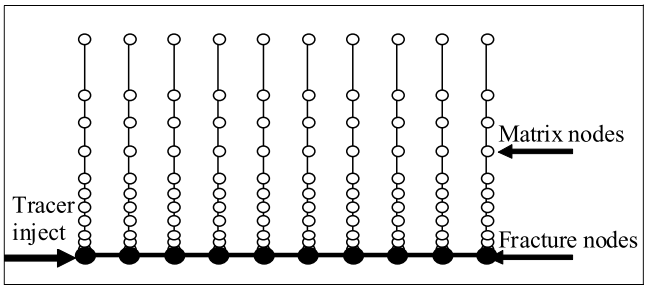

Figure 10. A conceptual illustration for the numerical grids of a generalized dual-porosity model. The fracture length L = 1000 m and the fracture aperture $2b$ = 0.002 m.

discretized into 10 nonuniform elements (whose sizes range from 0.001 to 0.4 m) with 11 nodes (the bottom matrix node is connected with the fracture node). This results in 10,010 matrix nodes. The initial concentration in the fracture is set to zero. At the first fracture node, the inflow water has a fixed injection rate of 0.0023 kg/s with a normalized uranium concentration of 1. The mean water residence time is about 10 days while the longitudinal dispersivity in fracture is assumed to be 10 m. The concentration breakthrough curves are computed at the last fracture node (node 1001).

[37] Ten thousand MC simulations are conducted for computing the concentration mean and variance at the last fracture node. The 10,000 realizations are sufficient to yield stable statistics. Figure 11a displays that the means and variances of MC simulations on three different days (160, 500, and 2000 days) at the last nodes converge between 4000 and 8000 realizations. Figure 11b, plotted according to equations (23) and (24) from *Ballio and Guadagnini* [2004], further shows that the coefficients of variations (CV) for the means and variances of 10,000 Monte Carlo simulations are less than 3%:

$$\mathrm{CV}_{\mathrm{mean}} = \frac{1}{\overline{C}_n}\sqrt{\frac{1}{n}\sum_{k=1}^{n}\left(\overline{C}_k - \overline{C}_{10,000}\right)^2} \tag{23}$$

$$\mathrm{CV}_{\mathrm{var}} = \frac{1}{\overline{S}_n}\sqrt{\frac{1}{n}\sum_{k=1}^{n}\left(\overline{S}_k - \overline{S}_{10,000}\right)^2}, \tag{24}$$

where $\overline{C}_n$ and $\overline{S}_n$ are the mean and variance of concentrations for n Monte Carlo simulations, respectively.

[38] The mean breakthrough curve of Monte Carlo simulations is plotted in the solid line in Figure 12. In order to assess the upscaling equations, one more GDPM simulation is implemented with the effective sorption coefficient and tortuosity derived in this study. Figure 12 shows that the breakthrough curve simulated with the effective sorption coefficient matches well with the mean concentration of the MC simulations. This result indicates that the effective sorption coefficient is an accurate estimate for the field-scale modeling. However, the computed concentration breakthrough curve using the effective sorption coefficient slightly underestimates the concentrations at the early time (from 50 to 300 days) when compared to the MC results. The MC results at early time also display larger variances than at later time (Figure 13). We believe that a contributing factor to the early time misfit in Figure 12 is that the MC simulations implicitly account for a small negative cross-correlation of $\tilde{R}_m$ and $\tilde{\tau}$, which is assumed to be 0 in the calculation of the effective mass transfer coefficient that was used in the single "effective" simulation. Even though $\tilde{R}_m$ and $\tilde{\tau}$ are randomly and independently generated for each of the three individual mineral facies (according to the parameters of Table 2), they actually have a small overall negative cross-covariance (~0.2) because of the slight negative correlation of the means and standard deviations of these parameters when considered collectively over all three mineral facies. A negative correlation results in a higher breakthrough curve at an early time because it implies that a larger $\tilde{R}_m$ or $\tilde{\tau}$ will tend to be offset by a smaller value of the other parameter, thus decreasing the tendency for larger values of the mass transfer coefficient that result in lower breakthrough curves. The higher breakthrough curve associated with a slight negative cross-covariance is reflected in the mean curve of the MC simulations in Figure 12, but not in the "effective" curve. Also, independent simulations confirmed that differences in breakthrough curves associated with different mass transfer coefficients are greater at an

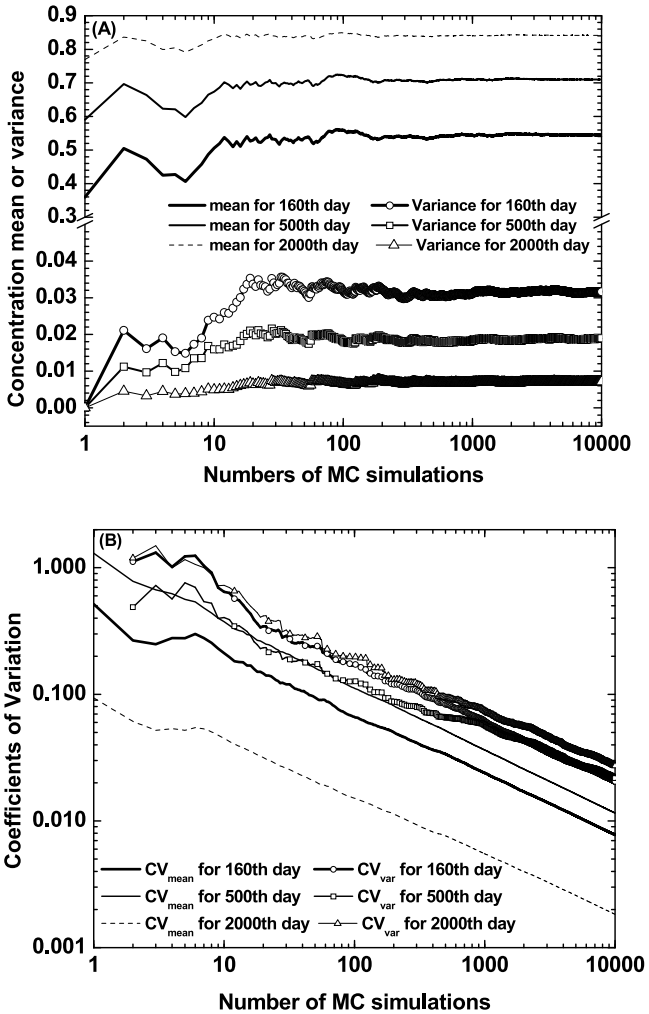

Figure 11. (a) The mean and variance and (b) coefficients of variations for the mean and variances change with the number of Monte Carlo (MC) simulations.

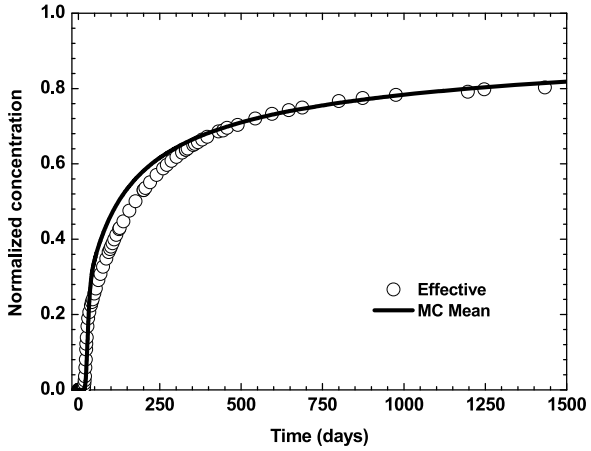

Figure 12. Comparison of normalized concentration breakthrough of MC simulations with that using the effective tortuosity and sorption coefficient.

earlier time, which is consistent with the greater variance of the MC breakthrough curves at early times in Figure 13.

[39] Another contributing factor to the early time misfit may be the temporal dependence of the mass transfer coefficient. As *Carrera et al.* [1998] and *Haggerty et al.* [2000] suggested, multiple first-order mass transfer rates were needed to exactly reproduce a diffusion process. However, because this study focuses on the spatial variations of the mass transfer coefficients, the upscaled tortuosity and retardation factor represent the averaging values of these parameters in the spatial and temporal domain. This averaging process may lead to the slight misfit at the early time and the good fit at the late time. The overall good match demonstrates that the upscaled effective parameters represent the physical and chemical characteristics of the heterogeneous domain.

6. Discussions

[40] The mass transfer coefficient between matrix and fracture is positively proportional to the square root of the product of the matrix tortuosity and retardation factor (equation (2)). Because the upscaled matrix tortuosity and retardation factor decrease as domain scale increases (equations (14) and (15)), the effective mass transfer coefficient must decrease with the increase of domain size. Figure 14 illustrates that the effective mass transfer coefficients increase with correlation scale of an indicator variable and decrease with the ratio of domain size to the indicator correlation scale. The latter is equivalent to decreasing the effective mass transfer coefficient as the domain size increases. *Reimus and Callahan* [2007] reported two orders of magnitude of decrease in mass transfer coefficients within a scale of a few hundred meters [*Reimus and Callahan*, 2007, Figure 4] based on data from transport experiments at the lab scale and tracer tests at the field scale. The trend of their results is consistent with our theoretical analysis, but with one order of magnitude difference. In their study, the fractures in the column experiments were different from those in field tracer tests. Except for the scaling effect, the relatively larger fracture apertures also contribute to the decreased mass transfer coefficients in field tracer tests.

[41] The scaling methodology developed in this paper may be extended to upscale weathering rates in modeling regional and global climate change [*Anderson et al.*, 2004] due to the equivalence between mass transfer coefficients and weathering rates in the fractured rock. Further study is needed to develop upscaling methods to obtain effective weathering rates, which can provide a more accurate prediction for chemical weathering, and thus lead to deeper insight into these processes and accumulated geochemical data.

[42] There are several limitations implicit in our results, which result from a simplified representation of the fracture-matrix system. Note that the upscaling methodology developed in this study is limited to the case of parallel fractures with constant apertures and at equal spacing, where the heterogeneous field of the matrix tortuosity is assumed to be independent of the retardation factor. Furthermore, it is implicit that the porosity variations have already been averaged out. In real fractured rock masses, additional complications arise due to the spatial variations of the aperture field within fractures, which leads to channeling and preferential transport, which will typically lead to more complex solute distributions in the rock matrix as well [*Neretnieks*, 2006]. Complexity of the fracture network topology is another factor that will require a more complex theoretical analysis. In realistic fractured rock masses that incorporate the above complexities, a more general approach to deriving effective transport parameters could involve starting from the local-scale governing equations in the fracture and matrix domains viewed as stochastic partial differential equations (due to the random fields of fracture aperture, matrix porosity, retardation, and tortuosity), and employing upscaling techniques such as those employed by *Gelhar* [1993] and *Cvetkovic et al.* [2007].

7. Summary and Conclusions

[43] The summary and conclusions drawn from this study are given below as follows.

[44] 1) The transition probability model and indicator geostatistics are used to characterize the physical and chemical heterogeneities, represented by matrix tortuosity

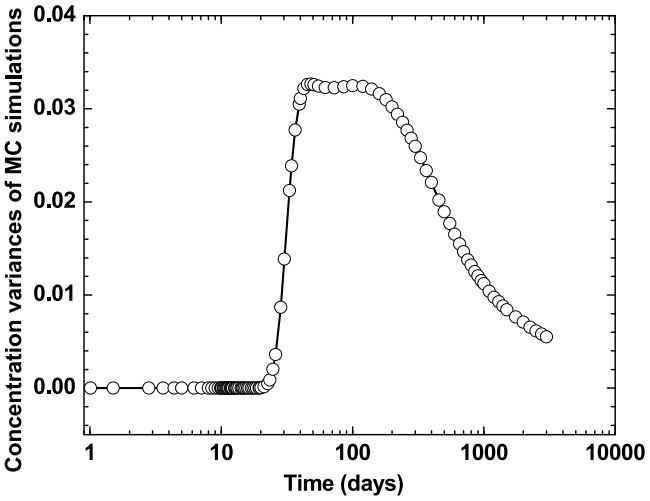

Figure 13. Evolution of the concentration variances through time.

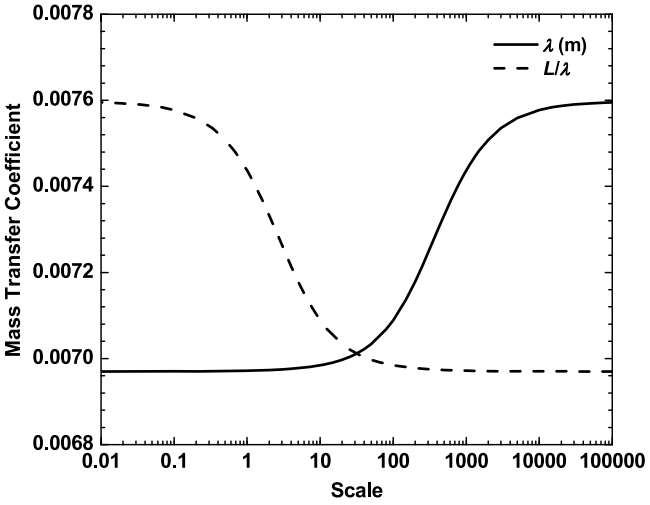

Figure 14. Effective mass transfer coefficient increases with correlation length of indicator variable (λ_I), in which the domain size keep constant (L = 1000 m) and decreases with the ratio of domain size to correlation length of indicator variable. The geometric mean of the mass transfer coefficient is 0.006.

and the retardation factor, within a framework of hierarchical-scale conceptual models of reactive mineral facies.

[45] 2) Upscaling equations for tortuosity and the sorption coefficient in fractured rocks with multimodal mineral facies are developed by volume averaging of mass transfer coefficients in the dual-porosity model. These equations demonstrate that the scale dependence of the reactive transport parameters is inherited from the spatial heterogeneity of the reactive mineral facies.

[46] 3) The effective sorption coefficient increases with correlation length of indicator variable, and with the integral scales and variances of retardation factor and tortuosity, but decreases with domain size.

[47] 4) The upscaling equations are verified by Monte Carlo simulations. The effective sorption coefficient developed in this study can be used to model linear sorption reactions for transport in heterogeneous fractured rocks. The upscaling equations provide accurate reactive transport parameters for field-scale modeling, which in turn results in better insight into contaminant transport and fate in fractured rocks, and thus is of practical significance.

[48] 5) The mass transfer coefficient for fractured rock is a function of the matrix tortuosity, the retardation factor, fracture aperture, and matrix porosity. The effective mass transfer coefficient decreases with increasing domain size like the effective tortuosity and retardation factor. Therefore, using column-scale mass transfer coefficients for calculating field-scale contaminant travel time may underpredict arrival time and make a site's long-term performance appear too favorable.

[49] **Acknowledgments.** This research is supported by Los Alamos National Laboratory's Directed Research and Development Project (number 20070441ER). We are grateful to Philip Stauffer, Kay Birdsell, and Mei Ding for their constructive comments on this manuscript. The editor Tissa Illangasekare, associate editor Harihar Rajaram, and the two anonymous reviewers are thanked for their insightful review of the manuscript.

References

Allen-King, R. M., R. M. Halket, D. R. Gaulord, and M. J. L. Robin (1998), Characterizing the heterogeneity and correlation of perchloroethene sorption and hydraulic conductivity using a facies-based approach, *Water Resour. Res.*, *34*(3), 385–396, doi:10.1029/97WR03496.

Allen-King, R. M., D. P. Divine, M. J. L. Robin, J. R. Alldredge, and D. R. Gaylord (2006), Spatial distributions of perchloroethylene reactive transport parameters in the Borden Aquifer, *Water Resour. Res.*, *42*, W01413, doi:10.1029/2005WR003977.

Anderson, S. P., et al. (2004), Proposed initiative would study Earth's weathering engine, *Eos Trans. AGU*, *85*(28), 265–272, doi:10.1029/2004EO280001.

Andersson, P., J. Byegard, E. L. Tullborg, T. Doe, J. Hermanson, and A. Winberge (2004), In situ tracer tests to determine retention properties of a block scale fracture network in granitic rock at the Aspo Hard Rock Laboratory, Sweden, *J. Contam. Hydrol.*, *70*(3–4), 271–297, doi:10.1016/j.jconhyd.2003.09.009.

Archie, G. E. (1947), Electrical resistivity an aid in core-analysis interpretation, *Am. Assoc. Pet. Geol. Bull.*, *31*(2), 350–366.

Ballio, F., and A. Guadagnini (2004), Convergence assessment of numerical Monte Carlo simulations in groundwater hydrology, *Water Resour. Res.*, *40*, W04603, doi:10.1029/2003WR002876.

Berkowitz, B., and H. Scher (1998), Theory of anomalous chemical transport in random fracture networks, *Phys. Rev. E*, *57*(5), 5858–5869, doi:10.1103/PhysRevE.57.5858.

Burr, D. T., E. A. Sudicky, and R. L. Naff (1994), Nonreactive and reactive solute transport in three-dimensional heterogeneous porous media: Mean displacement, plume spreading, and uncertainty, *Water Resour. Res.*, *30*(3), 791–815, doi:10.1029/93WR02946.

Carle, S. E. (1999), T-PROGS: *Transitional Probability Geostatistical Software, Users' Guide*, Univ. of Calif., Davis.

Carrera, J., X. Sanchez-Vila, I. Benet, A. Medina, G. Galarza, and J. Guimera (1998), On matrix diffusion: Formulations, solution methods, and qualitative effects, *Hydrogeol. J.*, *6*(1), 178–190, doi:10.1007/s100400050143.

Chao, C.-H., H. Rajaram, and T. H. Illangasekare (2000), Intermediate-scale experiments and numerical simulations of transport under radial flow in a two-dimensional heterogeneous porous medium, *Water Resour. Res.*, *36*(10), 2869–2884, doi:10.1029/2000WR900096.

Cushman, J. H. (1990), *Dynamics of Fluids in Hierarchical Porous Media*, Academic, San Diego, Calif.

Cushman, J. H., L. S. Bennethus, and B. X. Hu (2002), A primer on upscaling tools for porous media, *Adv. Water Resour.*, *25*, 1043–1067.

Cvetkovic, V., and G. Dagan (1994), Transport of kinetically sorbing solute by steady random velocity in heterogeneous porous formations, *J. Fluid Mech.*, *265*(1), 189–215, doi:10.1017/S0022112094000807.

Cvetkovic, V., S. Painter, N. Outters, and J. O. Selroos (2004), Stochastic simulation of radionuclide migration in discretely fractured rock near the Äspö Hard Rock Laboratory, *Water Resour. Res.*, *40*, W02404, doi:10.1029/2003WR002655.

Cvetkovic, V., H. Cheng, H. Widestrand, J. Byegård, A. Winberg, and P. Andersson (2007), Sorbing tracer experiments in a crystalline rock fracture at Äspö (Sweden): 2. Transport model and effective parameter estimation, *Water Resour. Res.*, *43*, W11421, doi:10.1029/2006WR005278.

Dai, Z., and J. Samper (2006), Inverse modeling of water flow and multicomponent reactive transport in coastal aquifer systems, *J. Hydrol. Amsterdam*, *327*(3–4), 447–461, doi:10.1016/j.jhydrol.2005.11.052.

Dai, Z., R. W. Ritzi, C. Huang, Y. N. Rubin, and D. F. Dominic (2004), Transport in heterogeneous sediments with multimodal conductivity and hierarchical organization across scales, *J. Hydrol. Amsterdam*, *294*(1–3), 68–86, doi:10.1016/j.jhydrol.2003.10.024.

Dai, Z., R. W. Ritzi Jr., and D. F. Dominic (2005), Improving permeability semivariograms with transition probability models of hierarchical sedimentary architecture derived from outcrop analog studies, *Water Resour. Res.*, *41*, W07032, doi:10.1029/2004WR003515.

Dai, Z., J. Samper, and R. Ritzi (2006), Identifying geochemical processes by inverse modeling of multicomponent reactive transport in Aquia aquifer, *Geosphere*, *2*(4), 210–219, doi:10.1130/GES00021.1.

Dai, Z., A. Wolfsberg, Z. Lu, and P. Reimus (2007a), Upscaling matrix diffusion coefficients for heterogeneous fractured rocks, *Geophys. Res. Lett.*, *34*, L07408, doi:10.1029/2007GL029332.

Dai, Z., A. V. Wolfsberg, Z. Lu, and R. W. Ritzi (2007b), Representing aquifer architecture in macrodispersivity models with an analytical solution of the transition probability matrix, *Geophys. Res. Lett.*, *34*, L20406, doi:10.1029/2007GL031608.

Dai, Z., A. V. Wolfsberg, Z. Lu, and H. Deng (2009), Scale dependence of sorption coefficients for radionuclide transport in saturated fractured rock, *Geophys. Res. Lett.*, *36*, L01403, doi:10.1029/2008GL036516.

Davis, J. A., S. B. Yabusaki, C. I. Steefel, J. M. Zachara, G. P. Curtis, G. D. Redden, L. J. Criscenti, and B. D. Honey (2004), Assessing conceptual models for subsurface reactive transport of inorganic contaminants, *Eos Trans. AGU*, *85*(44), 2, doi:10.1029/2004EO440002.

Fernàndez-Garcia, D., T. H. Illangasekare, and H. Rajaram (2005), Differences in the scale dependence of dispersivity and retardation factors estimated from forced-gradient and uniform flow tracer tests in three-dimensional physically and chemically heterogeneous porous media, *Water Resour. Res.*, *41*, W03012, doi:10.1029/2004WR003125.

Frampton, A., and V. Cvetkovic (2007), Upscaling particle transport in discrete fracture networks: 2. Reactive tracers, *Water Resour. Res.*, *43*, W10429, doi:10.1029/2006WR005336.

Gelhar, L. W. (1993), *Stochastic Subsurface Hydrology*, Prentice Hall, Englewood Cliffs, N. J.

Ginn, T. R. (1999), On the distribution of multicomponent mixtures over generalized exposure time in subsurface flow and reactive transport: Foundations and formulations for groundwater age, chemical heterogeneity, and biodegradation, *Water Resour. Res.*, *35*(5), 1395–1407, doi:10.1029/1999WR900013.

Haggerty, R., S. A. McKenna, and L. C. Meigs (2000), On the late-time behavior of tracer test breakthrough curves, *Water Resour. Res.*, *36*(12), 3467–3479, doi:10.1029/2000WR900214.

Hu, B. X., and H. Huang (2002), Stochastic analysis of solute transport in heterogeneous dual-permeability media, *Water Resour. Res.*, *38*(9), 1175, doi:10.1029/2001WR000442.

Huang, C., and Z. Dai (2008), Modeling groundwater in multimodal porous media with localized decompositions, *Math. Geosci.*, *40*, 689–704, doi:10.1007/s11004-008-9167-3.

Huang, H., and B. X. Hu (2001), Nonlocal reactive transport in heterogeneous dual-porosity media with rate-limited sorption and interregional diffusion, *Water Resour. Res.*, *37*(3), 639–747, doi:10.1029/2000WR900327.

Journel, A. G. (1983), Nonparameteric estimation of spatial distributions, *Math. Geol.*, *15*(3), 445–468, doi:10.1007/BF01031292.

Kwicklis, E. M., A. V. Wolfsberg, P. H. Stauffer, M. A. Walvoord, and M. J. Sully (2006), Multiphase, multicomponent parameter estimation for liquid and vapor fluxes in deep arid systems using hydrologic data and natural environmental tracers, *Vadose Zone J.*, *5*(3), 934–950, doi:10.2136/vzj2006.0021.

Li, L., C. A. Peters, and M. A. Celia (2007), Effects of mineral spatial distribution on reaction rates in porous media, *Water Resour. Res.*, *43*, W01419, doi:10.1029/2005WR004848.

Lichtner, P. C. (1993), Scaling properties of time-space kinetic mass transport equations and the local equilibrium limit, *Am. J. Sci.*, *293*(4), 257–296.

Liu, C., J. M. Zachara, N. P. Qafoku, and Z. Wang (2008), Scale-dependent desorption of uranium from contaminated subsurface sediments, *Water Resour. Res.*, *44*, W08413, doi:10.1029/2007WR006478.

Liu, H. H., Y. Q. Zhang, and F. J. Molz (2007), Scale dependence of the effective matrix diffusion coefficient: Some analytical results, *Vadose Zone J.*, *6*(3), 679–683, doi:10.2136/vzj2006.0140.

Lu, Z., and D. Zhang (2002), On stochastic modeling of flow in multimodal heterogeneous formations, *Water Resour. Res.*, *38*(10), 1190, doi:10.1029/2001WR001026.

Meile, C., and K. Tuncay (2006), Scale dependence of reaction rates in porous media, *Adv. Water Resour.*, *29*(1), 62–71, doi:10.1016/j.advwatres.2005.05.007.

Neretnieks, I. (2006), Channeling with diffusion into stagnant water and into a matrix in series, *Water Resour. Res.*, *42*, W11418, doi:10.1029/2005WR004448.

Neuman, S. P. (2005), Trends, prospects, and challenges in quantifying flow and transport through fractured rocks, *Hydrogeol. J.*, *13*, 124–147, doi:10.1007/s10040-004-0397-2.

Rajaram, H. (1997), Time and scale dependent effective retardation factors in heterogeneous aquifers, *Adv. Water Resour.*, *20*(4), 317–230, doi:10.1016/S0309-1708(96)00021-8.

Reimus, P. W., and T. J. Callahan (2007), Matrix diffusion rates in fractured volcanic rocks at the Nevada Test Site: Evidence for a dominant influence of effective fracture aperture, *Water Resour. Res.*, *43*, W07421, doi:10.1029/2006WR005746.

Reimus, P. W., G. Pohll, T. Mihevc, J. Chapman, M. Haga, B. Lyles, S. Kosinski, R. Niswonger, and P. Sanders (2003), Testing and parameterizing a conceptual model for solute transport model in fractured granite using multiple tracers in a forced-gradient test, *Water Resour. Res.*, *39*(12), 1356, doi:10.1029/2002WR001597.

Ritzi, R. W. (2000), Behavior of indicator semivariograms and transition probabilities in relation to the variance in lengths of hydrofacies, *Water Resour. Res.*, *36*(11), 3375–3381, doi:10.1029/2000WR900139.

Ritzi, W. R., Z. Dai, D. F. Dominic, and Y. N. Rubin (2004), Spatial correlation of permeability in cross-stratified sediment with hierarchical architecture, *Water Resour. Res.*, *40*, W03513, doi:10.1029/2003WR002420.

Robin, M. J. L., E. A. Sudicky, R. W. Gillham, and R. G. Kachanoski (1991), Spatial variability of strontium distribution coefficients and their correlation with hydraulic conductivity in the Canadian forces base Borden aquifer, *Water Resour. Res.*, *27*(10), 2619–2632, doi:10.1029/91WR01107.

Robinson, B. A. (1994), A strategy for validating a conceptual model for radionuclide migration in the saturated zone beneath Yucca Mountain, *Radioact. Waste Manage. Environ. Restor.*, *19*(1), 73–96.

Robinson, B. A., A. V. Wolfsberg, H. S. Viswanathan, and P. W. Reimus (2007), A colloid-facilitated transport model with variable colloid transport properties, *Geophys. Res. Lett.*, *34*, L09401, doi:10.1029/2007GL029625.

Rubin, Y. (1997), Transport of inert solutes by groundwater: Recent developments and current issues, in *Subsurface Flow and Transport: A Stochastic Approach*, edited by G. Dagan and S. P. Neuman, pp. 115–132, Cambridge Univ. Press, Cambridge, U. K.

Rubin, Y. (2003), *Applied Stochastic Hydrogeology*, 391 pp., Oxford Univ. Press, New York.

Samper, J., and C. Yang (2006), Stochastic analysis of transport and multicomponent competitive monovalent cation exchange in aquifers, *Geosphere*, *2*(2), 102–112, doi:10.1130/GES00030.1.

Scheibe, T. D., and D. L. Freyberg (1995), The use of sedimentological information for geometric simulation of natural porous media structure, *Water Resour. Res.*, *31*(12), 3259–3270, doi:10.1029/95WR02570.

Steefel, C. I., D. J. DePaolo, and P. C. Lichtner (2005), Reactive transport modeling: An essential tool and a new research approach for the Earth Sciences, *Earth Planet. Sci. Lett.*, *240*(3–4), 539–558, doi:10.1016/j.epsl.2005.09.017.

Stoller-Navarro Joint Venture (2009), Phase I transport model of corrective action units 101 and 102: Central and western Pahute Mesa, Nevada Test Site, Nye County, Nevada (draft), *Rep. S-N/99205-111*, Las Vegas, Nev.

Stumm, W., and J. J. Morgan (1995), *Aquatic Chemistry: Chemical Equilibria and Rates in Natural Waters*, 3rd ed., 1040 pp., John Wiley, New York.

Sudicky, E. A., and O. Frind (1982), Contaminant transport in fractured porous media: Analytical solution for a system of parallel fractures, *Water Resour. Res.*, *17*(3), 555–564.

Tang, D. H., E. O. Frind, and E. A. Sudicky (1981), Contaminant transport in fractured porous media: Analytical solution for single fracture, *Water Resour. Res.*, *18*(7), 1634–1642.

Tompson, A. F. B. (1993), Numerical simulation of chemical migration in physically and chemically heterogeneous porous media, *Water Resour. Res.*, *29*(11), 3709–3726, doi:10.1029/93WR01526.

Tsang, C.-F., and C. Neretnieks (1998), Flow channeling in heterogeneous fractured rocks, *Rev. Geophys.*, *36*(2), 275–298, doi:10.1029/97RG03319.

Wolfsberg, A. V., L. Glascoe, G. Lu, A. Olson, P. Lichtner, M. McGraw, T. Cherry, and G. Roemer (2002), TYBO/BENHAM: Model Analysis of Groundwater Flow and Radionuclide Migration from Underground Nuclear Tests in Southwestern Pahute Mesa, Nevada, *Rep. LA-13977*, 424 pp., Los Alamos National Laboratory, Los Alamos, NM.

Xu, T., J. Samper, C. Ayora, M. Manzano, and E. Custodio (1999), Modeling of nonisothermal multicomponent reactive transport in field-scale porous media flow systems, *J. Hydrol. Amsterdam*, *214*(1–2), 144–164, doi:10.1016/S0022-1694(98)00283-2.

Ye, M., and R. Khaleel (2008), A Markov chain model for characterizing medium heterogeneity and sediment layering structure, *Water Resour. Res.*, *44*, W09427, doi:10.1029/2008WR006924.

Zavarin, M., S. F. Carle, and R. M. Maxwell (2004), Upscaling Radionuclide Retardation-Linking the Surface Complexation and Ion Exchange Mechanistic Approach to a Linear Kd Approach, *Rep UCRL-TR-204713*, Lawrence Livermore Natl. Lab., Livermore, Calif.

Zhang, D., and Z. Lu (2004), An efficient higher-order perturbation approach for flow in randomly heterogeneous porous media via

Karhunen-Loeve decomposition, *J. Comput. Phys.*, *194*(2), 773–794, doi:10.1016/j.jcp.2003.09.015.

Zhou, Q., H.-H. Liu, F. J. Molz, Y. Zhang, and G. S. Bodvarsson (2007), Field-scale effective matrix diffusion coefficient for fractured rock: Results from literature survey, *J. Contam. Hydrol.*, *93*(1–4), 161–187, doi:10.1016/j.jconhyd.2007.02.002.

Zyvoloski, G. A., B. A. Robinson, and H. S. Viswanathan (2008), Generalized double porosity: A numerical method for representing spatially variable subgrid-scale processes, *Adv. Water Resour.*, *31*(3), 535–544, doi:10.1016/j.advwatres.2007.11.006.

Z. Dai, H. Deng, Z. Lu, P. Reimus, and A. Wolfsberg, Earth and Environmental Sciences Division, Los Alamos National Laboratory, EES-16, T003, Los Alamos, NM 87545, USA. (daiz@lanl.gov)

M. Ye, Department of Scientific Computing, Florida State University, 315 Keen Bldg., Tallahassee, FL 32306, USA.